Crystallographic studies of shikimate binding and induced conformational changes in *Mycobacterium tuberculosis* shikimate kinase

Balvinder Dhaliwal[a], Charles E. Nichols[a], Jingshan Ren[a], Michael Lockyer[b], Ian Charles[b], Alastair R. Hawkins[c], David K. Stammers[a,*]

[a] *Division of Structural Biology, The Wellcome Trust Centre for Human Genetics, University of Oxford, Roosevelt Drive, Oxford OX3 7BN, UK*
[b] *Arrow Therapeutics, Britannia House, 7 Trinity Street, London SE1 1DA, UK*
[c] *School of Cell and Molecular Biosciences, Catherine Cookson Building, Medical School, Framlington Place, University of Newcastle-upon-Tyne, Newcastle-upon-Tyne NE2 4HH, UK*

Received 1 June 2004; revised 7 July 2004; accepted 4 August 2004

Available online 13 August 2004

Edited by Hans Eklund

Abstract The X-ray crystal structure of *Mycobacterium tuberculosis* shikimate kinase (SK) with bound shikimate and adenosine diphosphate (ADP) has been determined to a resolution of 2.15 Å. The binding of shikimate in a shikimate kinase crystal structure has not previously been reported. The substrate binds in a pocket lined with hydrophobic residues and interacts with several highly conserved charged residues including Asp34, Arg58, Glu61 and Arg136 which project into the cavity. Comparisons of our ternary SK–ADP–shikimate complex with an earlier binary SK–ADP complex show that conformational changes occur on shikimate binding with the substrate-binding domain rotating by 10°. Detailed knowledge of shikimate binding is an important step in the design of inhibitors of SK, which have potential as novel anti-tuberculosis agents.

Keywords: Shikimate pathway; Shikimate kinase; Shikimate; X-ray crystallography; Drug design; Tuberculosis

1. Introduction

The shikimate pathway is a seven step biosynthetic pathway which converts phosphoenolpyruvate and erythrose 4-phosphate to chorismate [1]. Chorismate is the major branch point in the synthesis of vitamins E and K, folic acid, ubiquinone and the essential aromatic α-amino acids [1]. Intermediates also serve as substrates for other metabolic pathways. Shikimate kinase (SK) (E.C. 2.7.1.71) catalyzes the fifth step in the shikimate pathway; phosphoryl transfer from adenosine triphosphate (ATP) to shikimate, yielding shikimate-3-phosphate. The shikimate pathway is essential to higher plants, fungi, algae, bacteria [1] and apicomplexan parasites [2], but is absent in mammals. Therefore, this pathway is an attractive target for the development of herbicides [3], antimicrobial agents [4], and antiparasite agents [2]. *Mycobacterium tuberculosis* (*Mt*) is one of the six microorganisms that account for over 90% of infectious diseases, a leading cause of death worldwide. The World Health Organisation reports that more adults and adolescents die from *Mt* than any other single infection [5].

Several SK crystal structures have previously been determined. Known SK structures include the *Erwinia chrysanthemi* (*Erc*) SK, unliganded and an MgADP complex [6]; *Escherichia coli* (*Ec*) SK I, unliganded [7]; *Campylobacter jejuni* SK, unliganded (not published, PDB accession code 1VIA) and an *Mt*SK MgADP complex [8]. Preliminary NMR studies on *Aquifex aeolicus* SK have been reported [9]. However, no SK structure with bound shikimate has yet been published. The work presented here reports the crystal structure of *Mt*SK with bound shikimate and describes associated conformational changes in the protein. Such knowledge will be of use in the design of novel inhibitors of shikimate kinase that may have potential as anti-mycobacterial drugs.

2. Materials and methods

2.1. MtSK cloning, protein expression and purification

A synthetic gene for *Mt*SK based on the amino acid sequence reported by Gu et al. [10] was made by Blue Heron Biotechnology (Bothell, WA 98021, USA). The *Mt*SK gene was initially cloned into pUC19 and subsequently an *Nde*I–*Bam*HI fragment containing the gene was excised and ligated into pET17b. Expression of *Mt*SK was carried out in the *Ec* strain BL21(DE3) at 37 °C using 100 μg/ml ampicillin for selection and 0.2 mg/ml IPTG for induction.

Following cell harvesting, sonication and centrifugation the supernatant was chromatographed on a DEAE Sephacel column equilibrated with 50 mM potassium phosphate, pH 7.2, 150 mM NaCl and 1mM DTT. The flow-through was subjected to an ammonium sulfate cut (30% saturation). The precipitate was re-dissolved and loaded onto a Sephacryl S-300 column and the flow through collected. Active fractions were identified by enzyme assay [8], analyzed by SDS–PAGE, made 1.0 M in ammonium sulfate and further fractionated on a phenyl Sepharose column.

2.2. Crystallization, data collection and structure determination

Prior to crystallization, *Mt*SK was concentrated and buffer exchanged for 20 mM Tris–HCl, pH 7.4, 40 mM KCl, and 0.1% sodium azide using Vivascience Vivaspin centrifugal concentrators. Pooled concentrates were then filtered through Amersham NAP™ 25 columns and re-concentrated to 15 mg/ml.

* Corresponding author. Fax: +44-1865-287547.
E-mail address: daves@strubi.ox.ac.uk (D.K. Stammers).

Abbreviations: ADP, adenosine diphosphate; ATP, adenosine triphosphate; *Ec*, *Escherichia coli*; *Erc*, *Erwinia chrysanthemi*; *Mt*, *Mycobacterium tuberculosis*; SD, standard deviation; SK, shikimate kinase; TAD, torsion angle difference

0014-5793/$22.00
doi:10.1016/j.febslet.2004.08.005

Table 1
Statistics for crystallographic structure determination

Wavelength (Å)	1.5418
Space group	$P3_221$
Unit cell (Å)	$a = b = 63.7$, $c = 91.6$
Unit cell (Å) *for 1L4Y*	$a = b = 63.9$, $c = 92.1$
Resolution range (Å)	30.0 – 2.15
Observations	72 430
Unique reflections	12 270
Completeness (%)	99.9
$I/\sigma I$	22.4
R_{merge} [a]	0.075
Wilson B value	40.52
Outer resolution shell	
Resolution range (Å)	2.19–2.15
Unique reflections	606
Completeness (%)	100
$I/\sigma I$	3.5
R_{merge} [a]	0.644
Refinement statistics	
Resolution range (Å)	30.0–2.15
No. of reflections (working/test)	10 549/1256
R factor [b] ($R_{working}/R_{free}$)	0.218 (0.211/0.279)
No. of atoms (protein/water/others)	1216/119/42
rms Bond length deviation (Å)	0.0084
rms Bond angle deviation (°)	1.48
Mean B factor (Å^2) [c]	49/53/53/49
rms Backbone B factor deviation [d]	3.6

[a] $R_{merge} = \sum |I - \langle I \rangle| / \sum \langle I \rangle$.
[b] R factor $= \sum |F_o - F_c| / \sum F_o$.
[c] Mean B factor for main-chain, side-chain, water and other ligands (ADP, shikimate and chloride), respectively.
[d] rms Deviation between B factors for bonded main-chain atoms.

Using a protein solution consisting of 14 mg/ml *Mt*SK, 5 mM adenosine diphosphate (ADP), and 5 mM shikimic acid (Sigma) and/or 5 mM $MgCl_2$, an initial crystallization screen of 480 conditions was carried out by the sitting drop vapor diffusion method. 200 nl drop sizes (1:1 protein/precipitant ratio) were set up using a Cartesian robot [11]. Based on the results obtained, further larger scale optimization screens were set up. Crystals grew from 0.5 M lithium chloride, 0.1 M Tris–HCl, pH 7–9, and 10–20% (w/v) PEG of various average molecular weights (PEG 2000–8000). The best diffracting crystals grew in the absence of magnesium. The crystal morphology improved significantly using lower molecular weight PEG as precipitant. Crystals grown from PEG 2000 were found to be of sufficient quality for X-ray diffraction experiments.

Crystals of *Mt*SK were flash-cooled to 100 K and data collected using Cu Kα radiation ($\lambda = 1.5418$ Å) from a Rigaku RU200H rotating anode generator and a 30 cm MAR image plate. The data were processed using the HKL (version 1.96.1) suite of programs [12]. Data collection and refinement statistics are shown in Table 1.

The *Mt*SK crystals are of the same space group as previously reported by Gu et al. [8,10], but with a slight change in each unit cell length (Table 1). The *Mt*SK–MgADP binary structure (PDB accession code: 1L4Y) was used as a starting model in order to solve the ternary *Mt*SK structure by the CNS suite of programs [13]. Initially, two rounds of rigid-body refinement followed by simulated annealing were performed. Cycles of positional and individual B-factor refinement, with bulk solvent correction followed. The model was rebuilt to include water molecules and chloride ions using the molecular graphics program *O* [14]. Electron density maps showed unambiguous $F_o - F_c$ density for both ADP and shikimate, which were added to the model during the later stages of refinement. The shikimate molecule was built using the molecular modeling program HyperChem v7.0 (Hypercube, Inc). The CNS parameter and topology files for shikimate were generated using the Uppsala Software factory program XPOL2D [15].

2.3. Model analysis and identification of conformational changes

The *Mt*SK ternary model was evaluated using PROCHECK [16], which indicated that 93.3% of the final model's residues lie within the most favored regions of a Ramachandran plot and 6.7% within the additionally allowed regions [17].

To compare different SK complexes, the structures were overlaid using TOP3D [18]. Cα torsion angles for each residue '*i*', defined as the dihedral angle Cα($i-1$)–Cα(i)–Cα($i+1$)–Cα($i+2$), were examined for each *Mt*SK complex according to the methods described by Flocco & Mowbray [19]. Torsion angle differences (TAD) between the binary and ternary complexes were plotted using an EXCEL macro as ([TAD]/2 SD)^2, allowing significant TAD peaks to be observed clearly above the noise. The locations of hinges were found using the TCL script HINGEFIND [20] (partition value = 0.5 and maximum domains = 4), run and visualized with the graphics package VMD [21].

3. Results and discussion

3.1. The crystal structure

The overall *Mt*SK structure consists of a central five-stranded parallel β-sheet surrounded by eight helices [8]. As with most SKs, the enzyme belongs to the family of nucleoside monophosphate kinases [1,22], (Archea SKs, however, belong to the GHMP-kinase family [23]). *Mt*SK consists of three domains: (1) the CORE domain containing the five stranded parallel β-sheet and the P-loop (residues 9–17), which forms the binding site for nucleotides; (2) the LID domain (residues Gly112 to Asp124), which closes over the active site and has residues that are essential for the binding of ATP; (3) the substrate binding (SB) domain (residues Thr33 to Glu61), which functions to recognize and bind shikimate. See [6,8,24] for further details.

The *Mt*SK dead end ADP-shikimate ternary complex structure (this paper) consists of residues 2–166 with residues 114–115 removed from the model. Electron density for the first N-terminal residue was not observed, and residues 114–115 and the C-terminal residues 167–173 appear to be disordered. The model also contains 3 chloride ions, 119 water molecules, 1 ADP molecule and 1 shikimate molecule. The binding mode of ADP to *Mt*SK in the ternary complex is essentially the same as that reported by Gu et al. [8] for the binary complex.

3.2. Shikimate binding

Unambiguous difference electron density for a shikimate molecule was found in a region corresponding to the NMP binding site in NMP kinases near α-helices α2, α3 and the N-terminal end of α4 (Fig. 1A). The binding of shikimate in a crystal structure of a shikimate kinase, which should be of importance in the development of inhibitors against the enzyme, has not been previously reported.

The shikimate binding site is characterized by a generally hydrophobic surface together with a number of charged residues which project into the cavity. The lipophilic part of the pocket is formed by Pro11 (part of the P-loop), and the highly conserved residues Phe49, Phe57, Gly79, Gly80, Gly81, Pro118 and Leu119. The phenyl rings of Phe49 and Phe57 are separated by ~4.5 Å and are orientated such that a weak ring stacking interaction is formed.

Shikimate makes several key interactions with highly conserved residues within the binding pocket (Fig. 1A): (1) The carboxylate group of the shikimate forms strong hydrogen bonds and a salt-bridge with the guanidinum group of Arg136; (2) The carboxylate group of Asp34 forms another bidentate H-bond with the O12 hydroxyl group of shikimate (the shikimate atom label nomenclature is shown

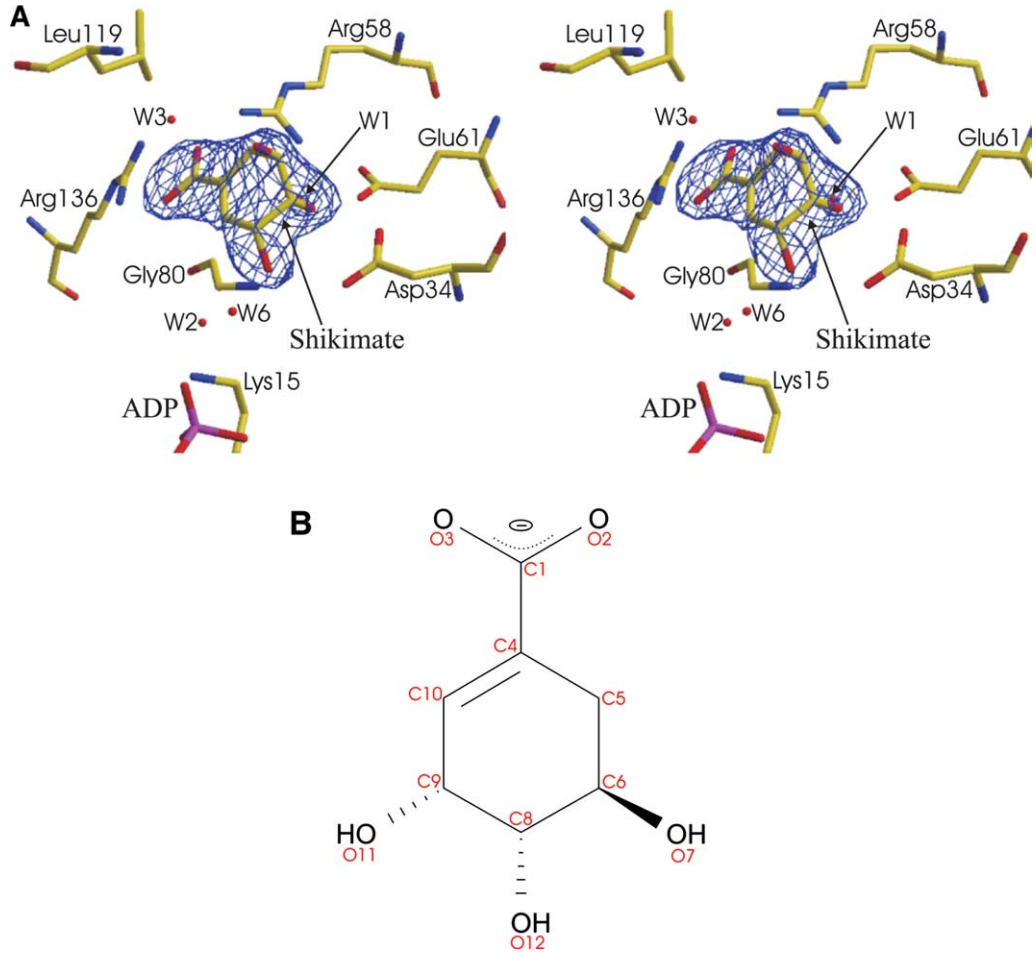

Fig. 1. The shikimate molecule. (A) Stereo diagram showing the $F_o - F_c$ annealed electron density map with shikimate omitted, contoured at 4.5σ. Also shown are the main interactions between the substrate, ordered water molecules and *Mt*SK. The figure was prepared using CNS [13], BOBSCRIPT [25] and Raster3D [26]. (B) Atom nomenclature for shikimate [27].

in Fig. 1B); (3) The NH2 atom of Arg58 forms a H-bond with the O2 atom group of the substrate; (4) The main-chain nitrogen of Gly80 interacts with the O11 hydroxyl group of shikimate.

Other highly conserved residues are observed to interact indirectly with the shikimate molecule: (1) Glu61 does not bind to the substrate directly as previously suggested [6], instead it interacts with the O12 hydroxyl of shikimate via a bridging water molecule,W1, which forms a 2.6 Å H-bond with the OE2 group of Glu61; (2) The main-chain nitrogen of Leu119 forms a 2.9 Å H-bond with the W3 oxygen atom, which in turn interacts with the O7 hydroxyl of shikimate; (3) the NZ atom of Lys15 forms a 2.6 Å H-bond with the oxygen atom of W2, which also interacts with the O11 hydroxyl of the substrate. Lys15 does not form a H-bond directly with shikimate, as previously suggested from a computational model of a MgADP-shikimate *Mt*SK complex [28]. Furthermore, the hypothetical model of *Mt*SK does not implicate Arg58, Glu61, Gly80 or Leu119 as being involved in shikimate binding to *Mt*SK as shown in this current work. The bridging water molecules in the active site are also present in the *Mt*SK binary complex [8]. A detailed list of contacts made between the shikimate molecule and *Mt*SK can be found in Table 2.

All of the interactions described above serve to position and orientate the O11 hydroxyl of the shikimate molecule ready for nucleophilic attack by the γ-phosphate of ATP.

3.3. Substrate induced conformational changes

In order to prevent unwanted ATP hydrolysis in the absence of substrate, kinases disassemble in the active site. The repositioning of catalytically critical residues is an induced fit movement resulting from the binding of substrate [6,24,29–33].

Previous studies have shown that adenylate kinases undergo a large conformational change during catalysis [31,34]. More recent reports have shown that conformational changes also occur in shikimate kinases during the catalytic cycle. Thus, circular dichroism studies have shown that *Erc*SK undergoes large conformational changes on the addition of ATP analogs or shikimate [6]. Indeed, a comparison of the apo *Erc*SK and ADP binary *Mt*SK structures has been used to suggest that significant conformational changes occur upon nucleotide binding [8]. It was proposed that ADP binding induces a large hinged movement of the LID domain over the active site, bringing Arg110 and Arg117 into positions essential for interaction with the nucleotide and about a 5 Å repositioning of the SB domain is observed.

Table 2
Interactions between *Mt*SK and shikimate

Shikimate atom	MtSK/water atom	Distance (Å)
C1	Gly81 N	3.3
	Arg136 NH1	3.4
	Arg136 NH2	3.5
	Wat5 O	3.6
C4	Wat1 O	3.5
	Wat3 O	3.5
C5	Wat1 O	3.4
	Wat3 O	3.5
C8	Asp34 OD2	3.4
	Asp34 CG	3.6
	Asp34 OD1	3.2
C9	Asp34 OD2	3.6
C10	Gly80 N	3.4
O2	Gly81 N	3.5
	Gly81 CA	3.5
	Arg136 CZ	3.5
	Arg136 NH1	3.5
	Arg136 NH2	2.8
	Arg58 NH2	2.6
	Leu119 CD1	3.1
O3	Pro11 CG	3.5
	Gly80 C	3.5
	Gly81 N	3.4
	Arg136 CZ	3.3
	Arg136 NH1	2.5
	Arg136 NH2	3.4
	Wat5 O	3.2
O7	Wat3 O	3.0
O11	Asp34 OD2	2.7
	Gly80 N	3.2
	Wat2 O	2.9
	Wat6 O	3.2
O12	Asp34 OD2	3.1
	Asp34 CG	3.2
	Asp34 OD1	2.6
	Gly79 CA	3.5
	Wat1 O	2.5

The distances were determined using the CONTACT program [18] with 0–3.6 Å distance limits.

In order to analyze any structural differences between the *Mt*SK complexes, the binary complex *Mt*SK-ADP structure was overlaid onto the ternary structure. A root-mean-square (rms) deviation of 0.7 Å for 164 pairs of Cα atoms (excluding residues 114–115) was calculated. The overlays were examined in *O* and it was found that the central CORE domains superimposed extremely well. When the Cα atoms of just the CORE domains were overlaid, the rms deviation was only 0.2 Å. However, conformational changes in the LID and SB domains were observed (Fig. 2). Overlaying the Cα atoms of just the LID (excluding residues 114–115) and SB domains from the two MtSK structures, the rms deviations were 1.5 and 0.4 Å, respectively. The conformational changes were further examined using TAD analysis.

During TAD analysis conformational changes can sometimes be difficult to resolve from the background 'noise', which can be attributed to coordinate error, differences in structure resolution, crystal contacts or flexible loops [19,35]. As the crystal contacts in the binary and ternary MtSK complex structures are essentially the same, these would have negligible effect on the TADs in this instance. *Mt*SK contains a large proportion of flexible loops which were initially removed in the TAD analysis to give a mean background of 3°. When the TAD analysis used the complete structures, the peaks could easily be resolved from background noise (Fig. 3). Analysis of the TAD plot and visualisation of the *Mt*SK models in VMD reveals that the movement of the peripheral SB and LID domains is controlled by two independent hinges [32]: (1) the SB hinge, involving a 10° counter-rotation of the SB and CORE domains about axis H1, with hinge points at Thr33 (HP1) and Gln55 (HP2) and (2) the LID hinge, involving a 6° counter-rotation of the LID and CORE domains about axis H2, with hinge points at Thr111 (HP3) and Pro123 (HP4). The net result is the movement of the SB and LID domains towards the bound shikimate (Fig. 2).

Shikimate binding induces domain closure, with the SB and LID domains moving inwards to complete the catalytically competent active site. It is unclear, however, whether the movements occur in a defined sequence or simultaneously. Combining the HINGEFIND data with TAD analysis of the binary and ternary models allows the identification of structural changes from four hinge points associated with α-helices α2, α4, α6 and α7.

When compared to the binary complex, the SB and LID domain movements in the ternary structure result in several key changes near the active site. Within the SB region, residue Arg58 is shifted 0.9 Å towards the carboxylate group of shikimate. Phe49 moves ~1.7 Å away from Phe57 and closer to the substrate. Phe57 translates towards the shikimate (with the CZ atom moving 1.2 Å) (Fig. 2B). The changes in the orientation and positions of phenylalanines 49 and 57 disrupt their strong ring stacking interactions and probably result from the van der Waals contacts of shikimate with both phenylalanines. In the LID domain, the sidechain of Arg117 is slightly reoriented (Fig. 2C), resulting in an H-bond of 2.6 Å in length between the oxygen atom of water molecule 6 and the NE atom of Arg117 (W6 also forms a 3.2 Å H-bond with the O11 hydroxyl of shikimate). Arg136 becomes more ordered in the ternary complex, adopting a single conformation that interacts with the shikimate carboxyl group, whilst in the binary complex with ADP it adopts two conformations.

The detailed stereochemistry of shikimate binding to *Mt*SK is revealed from the crystal structure reported here. The identification of domain and loop closure in *Mt*SK associated with shikimate binding demonstrates the importance of an experimentally determined structure, since significant differences from the earlier docking studies of shikimate binding to a model of *Mt*SK [28] have been shown. Knowledge of conformational changes resulting from substrate binding is clearly important in the use of structure based approaches to design novel inhibitors of the enzyme targeting the shikimate binding site. It is hoped that such inhibitors will eventually give rise to new anti-mycobacterial drugs.

4. PDB accession number

Coordinates have been deposited in the PDB with the accession code 1U8A.

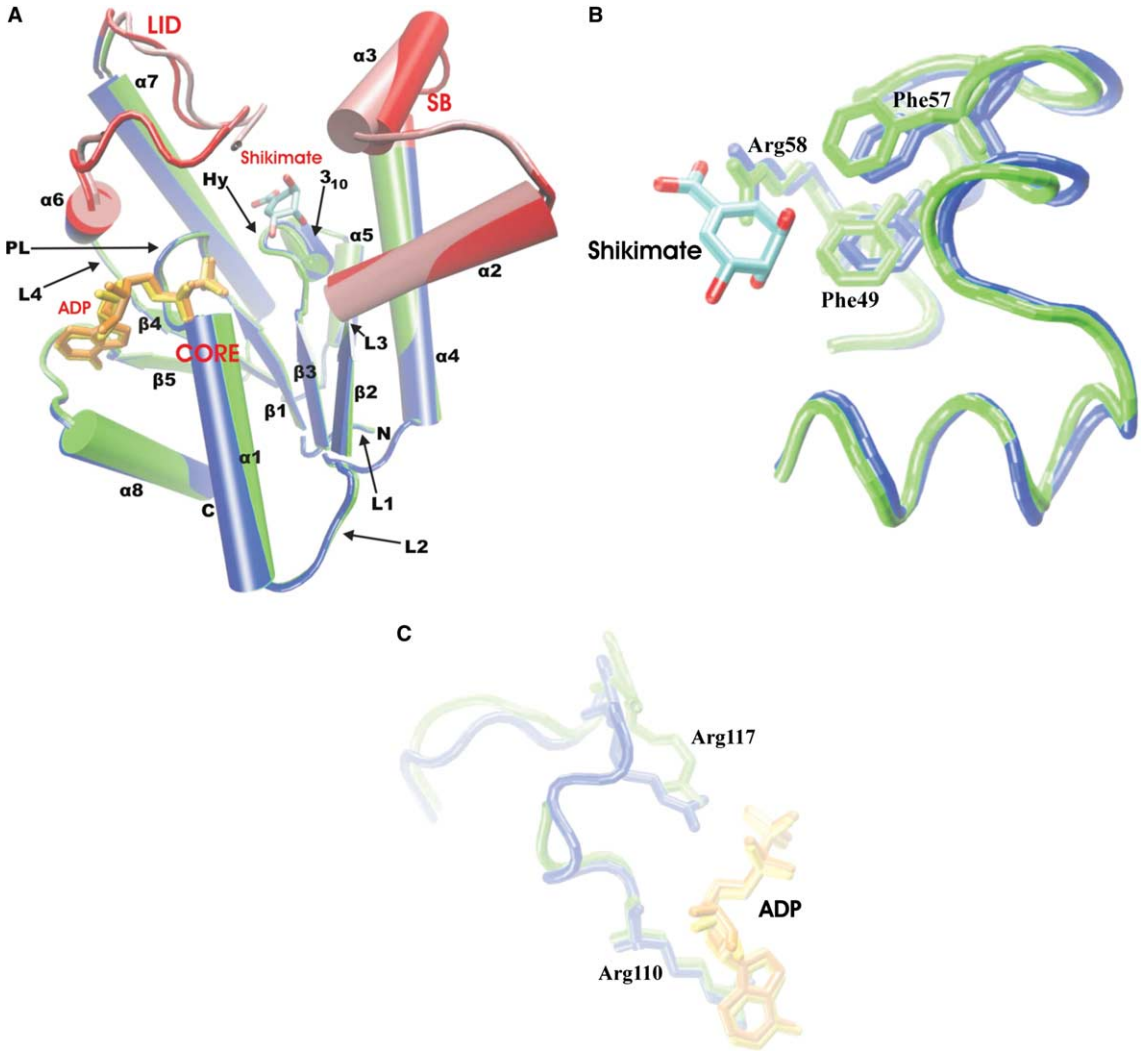

Fig. 2. The superimposed binary and ternary complexes of *Mt*SK. (A) Cartoon representation of the overall structure of *Mt*SK indicating the three domains; CORE, SB and LID, secondary structure elements, loop regions and bound ligands. The four pivot points, HP1-HP4, associated with shikimate induced conformational changes in SK are marked. (B) and (C) Tube representations of the *Mt*SK SB and LID domain overlays, respectively. The binary and ternary *Mt*SK structures are colored blue and green, respectively, except for the conformational differences in the SB and LID regions of the binary and ternary complexes, which are colored red and pink, respectively. The ADP molecules bound in the binary and ternary complexes are colored yellow and orange, respectively. (Residues 114–115 are excluded from the ternary complex.) The figures were prepared using VMD [21].

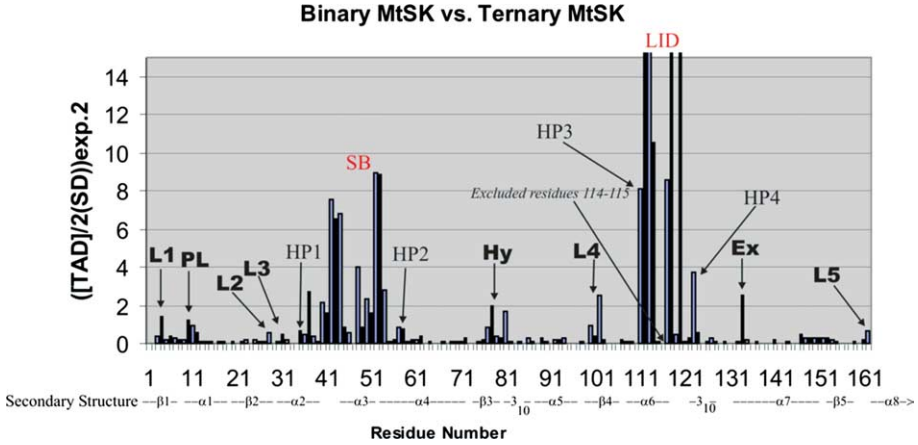

Fig. 3. Torsion angle difference plot for *Mt*SK between the binary and ternary complexes. The significant TAD peaks are labeled: SB, SB domain; LID, LID domain; L1, N-terminal loop; PL, P-loop connecting β1 to α1; L2, loop connecting α1 to β2; L3, loop connecting β2 to α2; L4, loop connecting β4 to α6; L5, C-terminal loop; Ex, Ala134 on the exterior of protein; Hy, Hydrophobic loop. The 4 hinge points are labeled HP1–HP4. Also depicted below the *x*-axis are the secondary structural elements of *Mt*SK.

Acknowledgements: We thank Dr. K. Harlos for assistance with the use of the X-ray facilities; Dr. R. Esnouf, Ms. J. Dong and Mr. A. Tamer for computer support. Work at Oxford and Newcastle was funded by Arrow Therapeutics.

References

[1] Hermann, K.M. and Weaver, L.M. (1999) Annu. Rev. Plant Physiol. Plant Mol. Biol. 50, 473–503.
[2] Roberts, F., Roberts, C.W., Johnson, J.J., Kyle, D.E., Krell, T., Coggins, J.R., Coombs, G.H., Milhous, W.K., Tzipori, S., Ferguson, D.J., Chakrabarti, D. and McLeod, R. (1998) Nature 393, 801–805.
[3] Kishore, G.M. and Shah, D.M. (1988) Annu. Rev. Biochem. 57, 627–663.
[4] Davies, G.M., Barrett-Bee, K.J., Jude, D.A., Nichols, W.W., Pinder, P.E., Thain, J.L., Watkins, W.J. and Wilson, R.G. (1994) Antimicrob. Agents Chemother. 38, 403–406.
[5] World Health Organisation (1999) Report on Infectious Diseases: Removing Obstacles to Healthy Development. Atar, Switzerland.
[6] Krell, T., Coggins, J.R. and Lapthorn, A.J. (1998) J. Mol. Biol. 278, 983–987.
[7] Romanowski, M.J. and Burley, S.K. (2002) Struct. Funct. Genet. 47, 558–562.
[8] Gu, Y., Reshetnikova, L., Li, Y., Wu, Y., Yan, H., Singh, S. and Ji, X. (2002) J. Mol. Biol. 319, 779–789.
[9] Liu, Q., Li, Y., Wu, Y. and Yan, H. (2000) J. Biomol. NMR 17, 277–278.
[10] Gu, Y., Reshetnikova, L., Li, Y., Yan, H., Singh, S.V. and Ji, X. (2001) Acta Crystallogr. D 57, 1870–1871.
[11] Walter, T.S., Diprose, J., Brown, J., Pickford, M., Owens, R.J., Stuart, D.I. and Harlos, K. (2003) J. Appl. Crystallogr. 36, 308–314.
[12] Otwinowski, Z. and Minor, W. (1997) Meth. Enzymol. 276, 307–326.
[13] Brünger, A.T., Adams, P.D., Glore, G.M., DeLano, W.L., Gros, P., Grosse-Kuntsleve, R.W., Jiang, J.S., Kuszewski, J., Nilges, M., Pannu, N.S., Read, R.J., Rice, L.M., Simonson, T. and Warren, G.L. (1998) Acta Crystallogr. D 54, 905–921.
[14] Jones, T.A., Zou, Y.-J., Cowan, S.W. and Kjeldgaard, M. (1991) Acta Crystallogr. A 47, 110–119.
[15] Kleywegt, G.J. and Jones, T.A. (1997) Meth. Enzymol. 277, 208–230.
[16] Lasowski, R.A., MacArthur, M.W., Moss, D.S. and Thorton, J.M. (1993) J. Appl. Crystallogr. 26, 283–291.
[17] Ramachandran, G.N., Ramakrishnan, C. and Sasisekharan, V. (1963) J. Mol. Biol. 7, 95–99.
[18] Collaborative-Computing-Project-4 (1994) Acta Crystallogr. D 50, 760–763.
[19] Flocco, M.M. and Mowbray, S.L. (1995) Protein Sci 4, 2118–2122.
[20] Wriggers, W. and Schulten, K. (1997) Proteins 29, 1–14.
[21] Humphrey, W., Dalke, A. and Schulten, K. (1996) J. Mol. Graph. 14, 33–38.
[22] Yan, H. and Ysai, M.-D. (1999) Advan. Enzymol. Relat. Areas Mol. Biol. 73, 103–134.
[23] Daugherty, M., Vonstein, V., Overbeek, R. and Osterman, A. (2001) J. Bacteriol. 183, 292–300.
[24] Krell, T., Maclean, J., Boam, D.J., Cooper, A., Resmini, M., Brocklehurst, K., Kelly, S.M., Price, N.C., Lapthorn, A.J. and Coggins, J.R. (2001) Protein Sci. 10, 1137–1149.
[25] Esnouf, R.M. (1999) Acta Crystallogr. D 55, 938–940.
[26] Merritt, E.A. and Bacon, D.J. (1997) Meth. Enzymol. 277, 505–524.
[27] Klotho: Biochemical Compounds Declarative Database. Available from http://www.biocheminfo.org/klotho/.
[28] Filgueira de Azevedo Jr., W., Canduri, F., Simões de Oliveira, J., Basso, L.A., Palma, M.S., Pereira, J.H. and Santos, D.S. (2002) Biochem. Biophys. Res. Commun. 295, 142–148.
[29] Jencks, W.P. (1975) Adv. Enzymol. 43, 219–410.
[30] Bennett, W.S. and Steitz, T.A. (1980) J. Mol. Biol. 140, 211–230.
[31] Schulz, G.E., Müller, C.W. and Diederichs, K. (1990) J. Mol. Biol. 213, 627–630.
[32] Idziak, C., Price, N.C., Kelly, S.M., Krell, T., Boam, D.J., Lapthorn, A.J. and Coggins, J.R. (1997) Biochem. Soc. Trans. 25, S627.
[33] Gerstein, M., Lesk, A.M. and Chothia, C. (1994) Biochemistry 33, 6739–6749.
[34] Müller, C.W., Schlauderer, G.J., Reinstein, J. and Schulz, G.E. (1996) Structure 4, 147–156.
[35] Zou, J., Flocco, M.M. and Mowbray, S.L. (1993) J. Mol. Biol. 233, 739–752.